and in order to ensure that the formwork is filled correctly, the minimum target workability class was set as F5, with no acceptance of any balls or indications of segregation.

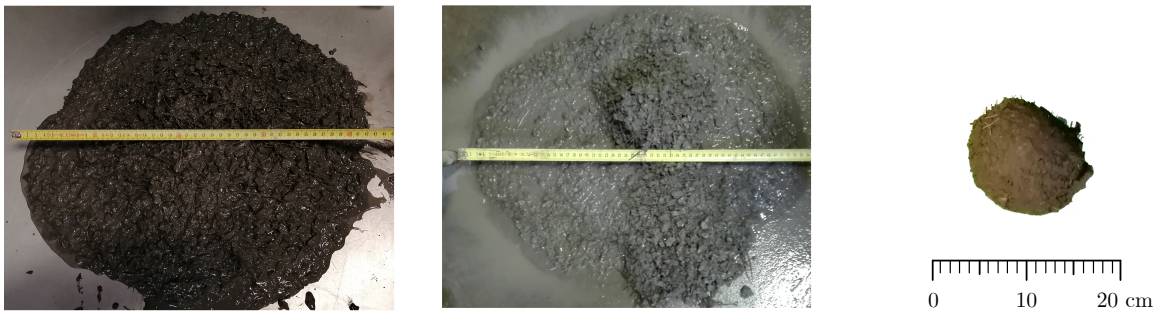

(a) (b) (c)

Figure 5.7: Results from the characterization of the workability of the mixes: (a) an acceptable spread, (b) a segregated spread, and (c) a ball of fibres and coarse aggregates.

Additional comments with respect to mix comparison can be added at this point. M2 had the lowest nominal flexural strength compared to M1 and M7, at the same V_f. The explanation lies in the incompatibility between the fibre type and the concrete mix, as small fibres (as the one used in M2, with a length of 13 mm) are designed for Ultra High-Performance Fibre Reinforced Concrete (UHPFRC). It is convenient to remind that, as a general rule of thumb, the fibre length should be three times the maximum aggregate size (DMax) [115]. However, M2 reached the highest flow diameter (600 mm in the flow table test). Due to the cost of the fibres M482, which are three times more expensive than the 4D+60, the use of these fibres for affordable coarse aggregate HPFRC is not recommended. The series M8 and M9 were cast looking for higher values of f_{R3k}. However, it was observed how the workability class was reduced from F3 to F2 compared with M7 with M8 when increasing the fibre content by 0.5%. M9 was discarded due to low workability and the appearance of fibre balls. Definitely, M1 was selected as the optimal mix when combining performance and cost.

5.4 Experimental testing

5.4.1 Introduction

The shear strength of the U-girder proposed in this research is highly dependent on the contribution of fibres; therefore, their distribution and orientation must be carefully controlled

to avoid the appearance of weak planes that would compromise the structural performance of the element. Consequently, the experimental campaign presented in the next sections is addressed at evaluating these issues considering the influence of concreting procedure, formwork shape, and concrete vibration on the tensile strength of the structural element. The experimental campaign consisted of 3 parts: prismatic specimens, L-shaped panels, and rectangular-shaped panels. These elements have different dimensions and are addressed at investigating different effects.

5.4.2 Prismatic specimens

This first stage of the experimental campaign was aimed at evaluating the effect of mould orientation during concreting and the location of planes between pours on the post-cracking flexural strength of the specimens. This study was done varying the waiting time between pours: 45 minutes and 3 hours. These values were selected as representative of a possible waiting time in a precast factory according to the authors' experience. The highest one (i.e., 3h) would be the consequence of a supply interruption during manufacturing.

The starting point of the experimental study was the fabrication of prismatic specimens to characterise the tensile strength of the concrete mix. The procedure followed the EN 14651 [4]: the prismatic mould was located horizontally upon a vibration table and filled to approximately 90% of the specimen height prior to the external compaction on the vibration table. Then, the mould was filled and screeded while compacting. The 13 notched prismatic specimens were cast following this method and tested to obtain the flexural strength for M1 which is considered as the reference series (H_{Ref}). Five additional series were cast, each consisting of 4 or 5 specimens, with variations in the position of the mould and concreting method. Two of these series were horizontally cast, while the remaining three were vertically cast. A vertical reference series (V_{Ref}) was cast without any discontinuous plane in the cross-section to be notched for comparison purposes. The other four series (the two horizontally cast (H_i) and the remaining vertically cast (V_i)) presented a potential weak plane at their mid height, which was formed by casting the specimens in two different layers and waiting a specific time between pourings to create a 'cold joint'. Two series presented a waiting time of 45 minutes (H_{45min}, V_{45min}), while the remaining two, 3 hours (H_{3h}, V_{3h}).

In the vertical series, the casting process was carefully controlled measuring the height of the bottom layer to locate the discontinuity on the notched section. It is worth mentioning that, after pouring, only a vibrating table was used without any poker vibrator to avoid breaking the 'cold joint' during concrete hardening.

All these specimens were tested in 3-point notched bending [4] and the average results are shown in Figure 5.8. The left part of the figure illustrates a zoom of the first part of the diagram to evaluate the concrete strength through the analysis of the limit of proportionality (f_L). The three horizontally cast series have almost the same f_L with a mean value and a coefficient of variation (CV) equal to 9.99 MPa (1.61%). In contrast, the vertically cast series present a mean value of 7.47 MPa (CV=58.55%). As main finding, it can be stated that the horizontal series reach the flexural strength of the concrete mix without any effect due to the existence of the 'cold joint'. In contrast, the vertically cast specimens present a significant reduction in the proportionality limit of the vertical specimens ($f_{L,V}$) due to waiting time between consequent pours; this phenomenon can be described with an exponential law (Equation 5.1), obtained through the minimum square adjustment method (R^2=0.97). In Equation 5.1 t is the waiting time between layers expressed in minutes.

$$f_{L,V} = 8.948e^{-0.003t[\text{min}]} \tag{5.1}$$

Regarding the post-cracking behaviour, the most notable aspect is that the horizontally cast series present an increase of the nominal strength compared to the pre-cracking scenario, while the vertically cast specimens shows a strong reduction. This phenomenon is numerically described by f_{R1m}/f_{Lm}: the horizontally cast series show a f_{R1m}/f_{Lm} with an average value of 1.74 (CV=2.75%), while the same result for the vertically cast series drops to 0.38 (CV=67.66%).

Furthermore, the f_{R1m} experiences similar results compared to the tensile strength of the concrete, represented by f_{Lm}, while the horizontally cast series are not affected by the waiting time, presenting the three series a f_{R1m} of 17.40 MPa (CV=2.92%). In contrast, the vertically cast specimens show a significantly lower average value of 3.12 MPa (CV=80.40%). The series V_{3h} has a f_{R1m}/f_{Lm}=0.10, which makes its post-cracking strength almost negligible. The post-cracking behaviour at ULS, which is numerically represented by f_{R3m}, indicates a reduction of 10% in the horizontally cast series, independent of the waiting time between pours. In contrast, in the vertically cast specimens, the f_{R3m} is significantly lower, leading to 3.58 MPa for V_{Ref} and V_{45min}.

This experimental campaign numerically proves that a relevant reduction f_{R1m} and f_{R3m} should be expected when prismatic specimens are cast in the vertical direction. This phenomenon was already pointed out by Mudadu et al. [116] who found reductions equal to 50% for f_{R1m} and 60% for f_{R3m}, if compared to the horizontally cast specimens. As explained by Edgington and Hannant [117], the phenomenon in question can be attributed

to the utilization of a vibrating table for the consolidation of concrete, which results in the alignment of fibres in the free surface plane, which is perpendicular to the primary direction of vibration; this leads to a reduction of the number of fibres crossing the 'notched section'. Furthermore, this effect might increase when the direction of vibration coincides with the direction of gravity. In this study, a similar effect is experimentally observed, with a reduction equal to 68.61% and 76.32% for f_{R1m} and f_{R3m}, respectively. Another important conclusion observed for the prismatic specimens under investigation was that a waiting time of 45 minutes does not cause a cold joint. However, a waiting time of 3 hours leads to the loss of post-cracking strength of the HPFRC, as observed in the series V_{3h}.

In case of a long waiting time between pours, a poker vibrator should be used to stitch the layers and distribute the fibres across the horizontal planes between the layers, minimising the potential post-cracking strength reduction due to the lack of crossing fibres. However, it should be checked that the poker vibrator does not leave holes in the concrete when dealing with waiting times of 3 hours.

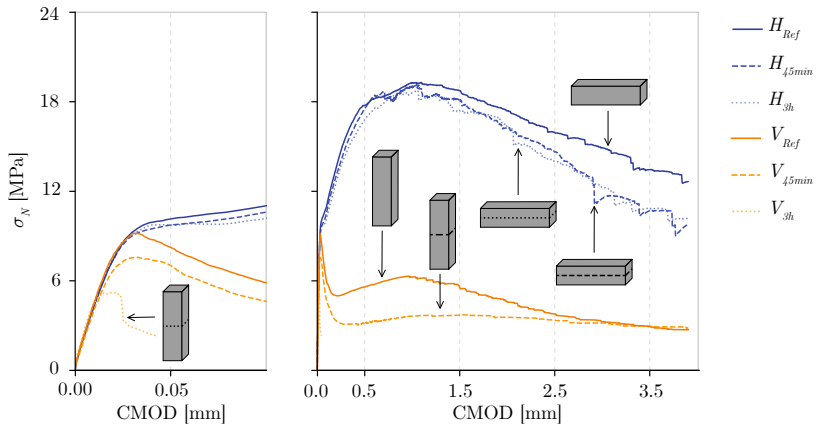

Figure 5.8: Average curves from the 3 point-bending tests of the specimens cast in different directions and with or without potential 'cold joints'.

5.4.3 L-shaped panels

The second part of the experimental campaign involved the construction of L-shaped panels aimed at replicating the web-bottom flange connection in the U-girder of the reference bridge (refer to Figure 5.1 (b)). This specimen consists of half of the U-girder bottom slab, its corner, and a part of the web. A schematic drawing of the formwork used for the U-girder, along with the cross-section of the U-girder, is shown in Figure 5.9 (a) (left). The idea

is to use conventional formworks to fabricate the U-girders, reducing the precasters initial investment in implementing the HPFRC technology. To follow the conventional concreting technique of casting the girder in longitudinal layers with a specific waiting time between them, the bottom slab was left open. The critical phase of this technique is the concreting of the second layer and the internal vibration of the plane between the first and second layers. The waiting time between pours must be minimized to reduce the loss of tensile strength previously described, but it should be sufficient to achieve enough strength of the bottom slab to withstand the pressure of the concrete poured in the second layer and the internal vibration.

The cross-section of the L-shaped specimen is presented in the right part of Figure 5.9 (a). The concreting of this specimen was performed in three layers: the first layer corresponded to the slab, the second and third to the web. The actual dimensions of the bridge U-girder were replicated, including the thickness of the bottom slab and web, which were 120 mm and 150 mm, respectively, and the height of the second and third layers were equal to 500 mm.

Two specimens were cast and tested in this experimental campaign. The first was produced by applying a waiting time between the pourings of the first and second layers of 45 minutes. This leads to the liquefaction of the first layer during the internal vibration of the second layer, as can be appreciated by the detail of Figure 5.9 (b). Based on this result, the waiting time for the equivalent phase of the second L-shaped panel was increased to 90 minutes. The second panel was successfully cast, and no liquefaction was observed. However, the bottom slab increased by 1 cm its thickness. As the main finding, a waiting time between pourings of 90 minutes was taken as an acceptable solution. This interval was used during the third stage of the experimental campaign involving the fabrication of rectangular-shaped panels to simulate the U-girder webs.

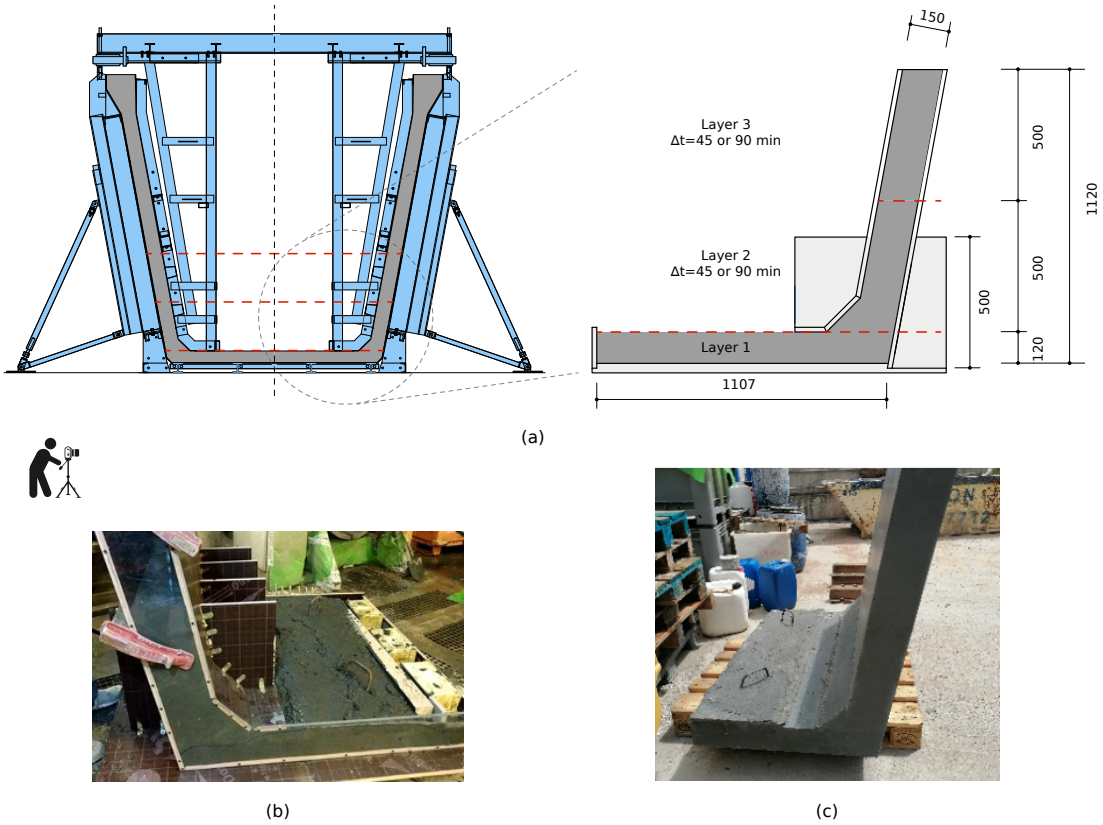

Figure 5.9: Description of the L-shaped panels: (a) left part: cross-section of the precast U-girder, in a schematic drawing of its formwork; right part: cross-section of the L-shaped panel (b) detail of the liquefied bottom slab when using a waiting time of 45 minutes between pourings, and (c) second L-shaped panel characterised by a waiting time of 90 minutes.

5.4.4 Rectangular-shaped panels

The third part of the experimental campaign consisted in executing two rectangular-shaped panels to replicate the U-girder webs. Figure 5.10 (a) shows their geometry, common to both panels, to increase the number of the data set and to obtain a certain degree of repeatability in the results. The panels have a thickness of 150 mm equal to the thickness of the U-girder web (b_w). The casting of each panel was based on four concrete batches. The discontinuity planes between concrete layers are marked with dashed lines, red when there was a waiting time between the concrete pouring of two consecutive layers, and blue when the pouring was executed in a continuous way. The waiting time between pourings was fixed at 90 minutes as discussed in the previous section with the L-shaped specimens. Furthermore, 6ϕ16 fibreglass

bars were placed with a 50 mm spacing in the bottom part of the panels (refer to Figure 5.10 (a) left) to simulate the typical arrangement of the prestressing steel strands. These bars were introduced within the panels to study how the HPFRC behaves with the presence of these obstacles, how steel fibres distribute around the strands and to detect potential obstruction due to the high content of long fibres together with the coarse aggregates. Together with each rectangular-shaped panel, 3 cylindrical and 5 prismatic specimens were cast to characterize, respectively, the compressive [114] and the post-cracking bending strength [4].

After hardening, several specimens were extracted from both panels. Figure 5.10 (a) illustrates the location of these 24 prismatic specimens (150x150x600 mm) and marks with different colours their orientation: vertical in orange, diagonal in green, and horizontal in purple. The specimens crossed by a pouring discontinuity are brighter in colours than the others. The results of the 3-point bending tests obtained from these specimens according to EN-14651 [4] provide insight into the distribution and orientation of the fibres and allow to evaluate the distribution coefficient of the fibres. Furthermore, the yellow specimens taken from the bottom were planned to be analysed by CT to obtain the distribution of the fibres and aggregates.

During the casting process, it was determined that the high viscosity of the concrete and the presence of fibres obstructing the concrete flow necessitated the application of vibration to facilitate flow from the container to the formwork. Upon placement of the HPFRC into the formwork, a poker vibrator was utilized to attain a uniform level of each layer. Figure 5.10 (b) shows a comparative illustration of the horizontal plane prior to (top) and after vibration (bottom). The pre-vibration image exhibits an accumulation of concrete towards one side of the formwork. However, the post-vibration image illustrates a horizontally levelled surface. The subsequent layers were poured by introducing the vibrator well beneath the discontinuity plane of the previously poured layer, with the objective of creating continuity of fibres along these planes. The pouring procedure involved a two-person operation wherein one worker operated the crane suspending the container, while the other worker operated the poker vibrator. The panels were created with a time gap of 2 weeks between them, and the sole difference between the two was the manner in which the concrete was poured into the formwork. Panel 1 was produced with a slope structure located under the container's opening, which was achieved using the web of a UPN steel beam. In contrast, panel 2 was cast without any additional structure, and the concrete was poured directly from the top of the formwork. The final aspect of the panel revealed solely marks left by the wooden formwork without any discernible indications of discontinuity.

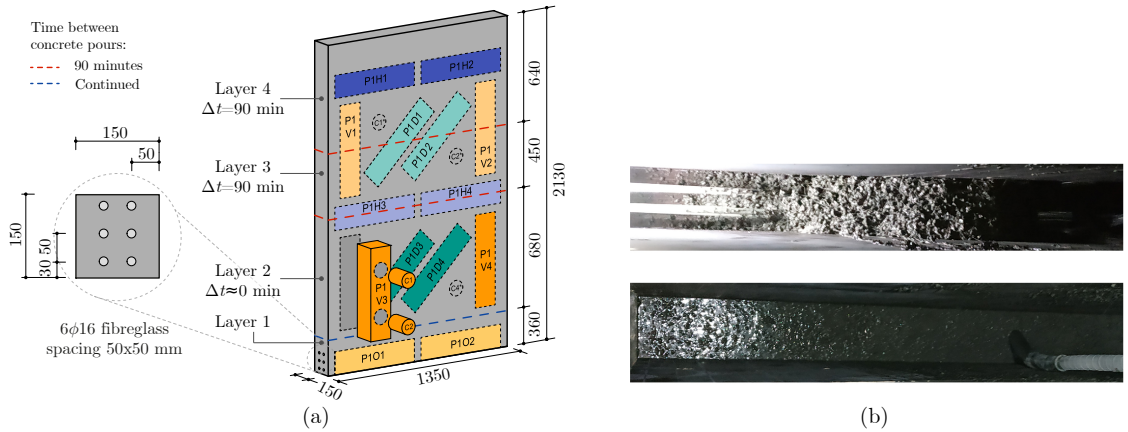

Figure 5.10: Third part of the experimental campaign based on rectangular-shaped panels: (a) panel geometry, casting process, and location of the prismatic specimens extracted, (b) top: a horizontal plane before the internal compaction, and bottom: after the internal compaction.

Figure 5.11 shows all the curves of the 3-point bending tests (experimental crack mouth opening displacement (CMOD) versus the nominal strength). Each row of figures is related to one of the two panels. Additionally, each column illustrates the specimens with a specific orientation (i.e., horizontal, vertical, and diagonal). Each plot shows the curves obtained from the 4 specimens extracted from the panels. For the readers' convenience, the same colour code is kept, and the location of each sample within the panel is shown. The curves obtained from the tested reference prismatic specimens are depicted in the corresponding graph in light grey, while their average curve is marked with a darker and thicker line. For the prismatic specimens, all numerical results in terms of f_L and $f_{R,j}$ are collected in Table 5.4.

Table 5.4: Values of f_L and $f_{R,j}$ from each of the prismatic specimens extracted from the panels.

Specimen ID	Pouring	Panel 1	Panel 2	Panel 1	Panel 2	Panel 1	Panel 2	Panel 1	Panel 2
		f_L	f_L	f_{R1}	f_{R1}	f_{R2}	f_{R2}	f_{R3}	f_{R3}
[-]	[-]	[MPa]	[MPa]	[MPa]	[MPa]	[MPa]	[MPa]	[MPa]	[MPa]
H3	Discont.	9.02	8.63	9.70	15.00	11.38	17.44	7.48	13.54
H4	Discont.	10.50	8.25	17.13	9.53	17.86	5.48	12.21	3.37
H1	Cont.	9.23	8.42	14.12	8.39	15.65	8.05	10.36	3.80
H2	Cont.	9.81	8.00	12.64	5.81	11.55	5.68	4.44	3.02
V1	Discont.	9.05	8.45	9.72	12.45	11.04	13.21	8.65	10.25
V2	Discont.	8.54	7.92	7.64	9.48	9.59	10.43	7.47	9.39
V3	Cont.	8.32	9.48	7.32	7.47	7.68	8.11	6.73	5.91
V4	Cont.	9.88	8.55	17.79	11.15	15.12	11.47	10.20	7.10
D1	Discont.	8.49	7.95	10.81	7.85	11.31	7.44	8.19	6.85
D2	Discont.	9.48	8.18	12.21	5.70	13.98	7.36	9.89	5.85
D3	Cont.	10.51	8.33	9.15	6.89	9.04	7.19	8.55	4.74
D4	Cont.	9.46	5.25	13.53	12.67	14.90	11.36	10.43	6.36
Mean value [MPa]		9.36	8.12	11.81	9.37	12.43	9.44	8.72	6.28
CV [%]		7.80	12.25	28.84	31.29	24.60	36.98	23.73	46.27
Charact. value [MPa]		7.85	6.06	4.78	3.31	6.11	2.23	4.44	0.29

The compressive strengths (f_{cm}) obtained from testing the three reference cylinders for panels 1 and 2 were, respectively, 131.40 (CV=3.56%) and 128.04 MPa (CV=5.54%). Furthermore, the prismatic specimens of the reference series from the two different panels show a maximum difference between the average curves from both panels of 0.69 MPa, which means a difference of 6.9% for the average curve obtained from both panels, from f_L until f_{R3}. This difference increases to 2.17 MPa (22.6%) because one test from panel 1 completely lost its post-cracking strength approximately at CMOD=2.5 mm. The concrete's batches of both panels presented similar mechanical strengths because the highest difference in their post-cracking flexural behaviour is 6.9% (CMOD=0.05-2.4 mm), and a difference of their f_{cm} is just 2.6%.

The 24 prismatic specimens extracted from the panels show a f_{Lm}=8.74 MPa (CV=9.38%), which is 10% lower than the f_{Lm}=9.64 MPa (CV=12%) of the reference specimens. However, this difference is accentuated in the post-cracking strength, f_{R1m} is equal to 10.59 MPa (CV=32%) and 15.70 MPa (CV=20%), and f_{R3m} is equal to 7.70 MPa (CV=36%) and 10.72 MPa (CV=48%), for the specimens extracted from the panels and from the reference specimens, respectively. Therefore, as main finding, a reduction in post-cracking strength of around 30% is observed in f_{R1m} and f_{R3m} of the specimens extracted from the panels

compared to the reference specimens.

Regarding the comparison between both panels, the specimens extracted from panel 2 present a lower bending post-cracking strength. These differences range from 1.24 MPa at f_{Lm} to 2.99 MPa at f_{R2m}. These values imply differences of 14% and 27%. The only difference between the two panels was the height at which the concrete was poured. A further experimental campaign should be carried out to identify stronger evidence to evaluate this effect and to define the maximum pouring height to not cause any reduction in the bending post-cracking strength.

From the prismatic specimens individually cast at the first stage of this experimental campaign (Subsection 5.4.2), a reduction in post-cracking strength of 70% was found when the specimens were cast in a vertical position instead of a horizontal one. This reduction was not found in the analysis of the results of the specimens extracted from the panels. In fact, the average f_{R1m} is 11.54 MPa and 10.38 MPa for the specimens extracted from the panels in horizontal and vertical positions, respectively. Regarding the f_{R3m}, it is equal to 7.28 MPa and 8.21 MPa for horizontally and vertically cast specimens, respectively. These differences, +10.6% and -12.0%, show no clear dependency between the post-cracking strength of the specimens and their orientations within the panel. Furthermore, by analysing the results from the vertically oriented specimens extracted from the panels, no effect due to the cold joint was detected. The average f_{R3m} for the specimens crossed by the joint is 8.94 MPa while it is lower, 7.49 MPa, for the other vertically oriented specimens without joint. Considering that the vertically oriented specimens crossed by the joint present a f_{R3m} 17.7% higher than the vertically oriented specimens without joint, it can be concluded that, fibres cross the planes between concrete layers thanks to the internal compaction with a poker vibrator.

Additionally, the average nominal strengths of the specimens with the same orientation (H, V and D) extracted from the panels are: $f_{R1m,H}$=11.54 MPa, $f_{R1m,V}$=10.38 MPa, and $f_{R1m,D}$=9.85 MPa; regarding f_{R3m} the values are: $f_{R3m,H}$=7.28 MPa, $f_{R3m,V}$=8.21 MPa, and $f_{R3m,D}$=7.61 MPa. Considering that the CV [%] for these three series are, for f_{R1m} and f_{R3m}, 8.2% and 6.2%, and the difference between the maximum and minimum f_{R1m} is 17.1% ($f_{R1m,H}$ is the maximum), and 12.8% for f_{R3m} ($f_{R3m,V}$ is the maximum), it can be concluded that the orientation of the specimens within the panels does not clearly influence its post-cracking strength.

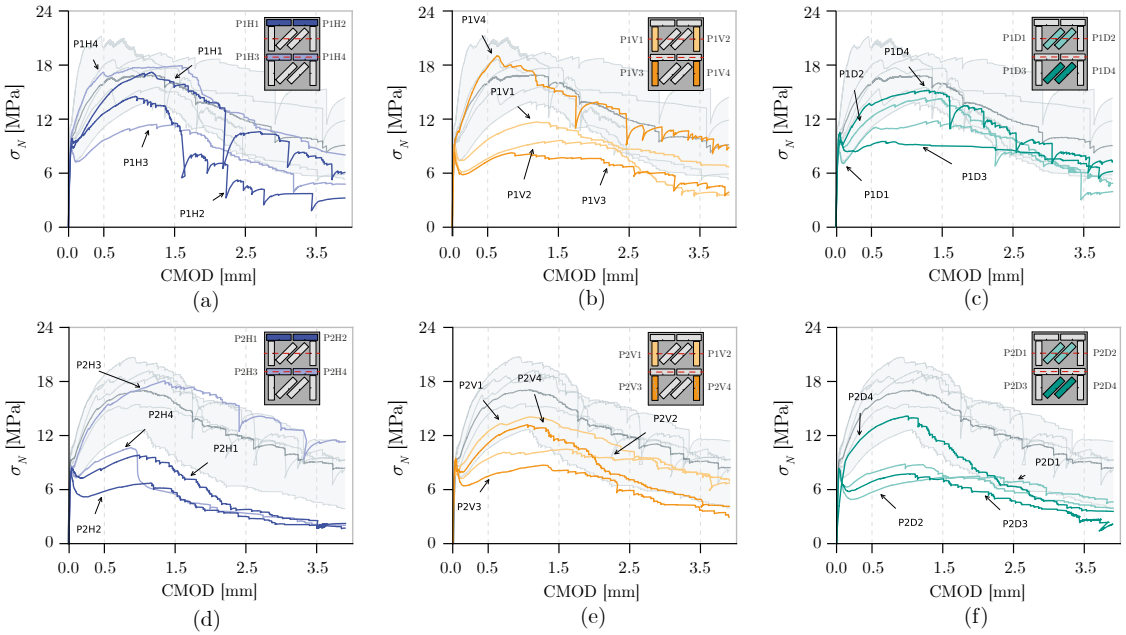

Figure 5.11: Third part of the experimental campaign based on rectangular-shaped panels: (a-f) curves crack mouth opening displacement (CMOD) versus the nominal strength of the 3 point bending tests.

5.4.5 Distribution and orientation of fibres

Further analyses were performed to assess the distribution and orientation of fibres in the hardened concrete elements. First, a digital image analysis of a section close to the notched section was applied to the 24 specimens extracted from both panels. Previous publications applying this method are found in other works [107] and [118]. To prepare the sample, the tested specimen was transversely sawed at a distance less than 20 mm from the notched section, and the section of analysis was cleaned with a brush to remove any trace of dust particles. The sample was placed in a darkened room, with the digital camera positioned at 90 cm from the section selected for analysis. The fibres reflect light, as can be observed in one of the photographs of specimen P2D1 shown in Figure 5.12 (a). However, it was found that, depending on the position and angle of the spotlight, only some fibres were detectable. Therefore, a sequence of photographs was taken from different positions and angles of the spotlight. Afterwards, using the Python extension Skimage, a threshold was applied to the photographs to remove noise identified as small reflections. Subsequently, all the photographs were joined together as a unique matrix, which can be seen in Figure 5.12 (b). The detection and collection of the characteristics of each particle of the figure was carried out specifically

performed with Skimage. The location, area, and maximum and minimum diameters were collected in a different matrix separated into 9 quadrants. According to Krenchel [119] the angle with respect to the surface under analysis is obtained as the arccosine between the minimum and maximum diameter of the particle. Fibres will provide a higher strength when it is perpendicular to the surface (φ=0º), while their strength is considered negligible when the angle is higher than 60º. The results of particle (fibre) counting and the average angle of inclination of the fibres are shown in Figure 5.12 (c) for each quadrant. The fibres of three specimens were manually counted to assess the accuracy of the method. It should be mentioned that these fibres are perfectly detectable with the naked eye. Figure 5.12 (d) showed how each fibre was numbered in quadrants and marked with a red marker. The digital counting method was able to detect on average 6% fewer fibres than manual counting. The reason is associated to the fact that groups of fibres are counted as one fibre by the digital method. In an attempt to reduce the difference, a method based on the watershed feature Skimage was implemented. However, it was disregarded because the scatter of the difference between the fibres counted by hand and the ones obtained by the digital method increased. Furthermore, the digital method accounted for a higher number of fibres than the real ones.

Figure 5.13 (a) shows the location of each fibre of the specimen P2D1. Furthermore, on the right is a histogram of the number of fibres in different horizontal strips. The upper 25 mm shown with a discontinuous line on the histogram the expected location of the neutral axis at CMOD=0.5 mm (f_{R1} condition), when the stress profile provided in the MC2010 is applied to the sectional equilibrium [49]. The fibres that contribute to the bending strength are expected to be those below the neutral axis. In addition, the orientation number η_φ, which is the average orientation of the fibres in the section, was calculated according to Schönlin [120] with Equation 5.2:

$$\eta_\varphi = \frac{1}{n}\sum_{i=1}^{n} cos\varphi_i \tag{5.2}$$

Where n is the number of fibres in the section and φ is the angle with respect to the plane of analysis. According to Schönlin [120], if the fibres are uniformly distributed: $\eta_{\varphi,1D}$=1, $\eta_{\varphi,2D}$=0.78, and $\eta_{\varphi,3D}$=0.66. Furthermore, the number of fibres theoretically expected in a section (N_{th}) can be obtained by Equation 5.3:

$$N_{th}[\text{fibres/cm}^2] = \frac{V_f}{A_f}\eta_\varphi = \frac{V_f}{\frac{\pi {D_f}^2}{4}}\eta_\varphi = \frac{V_f}{\frac{\pi 0.75^2}{4}}\eta_\varphi = 2.26\eta_\varphi \tag{5.3}$$